Electronic Supplementary Material (ESI) for Nanoscale.

Supplementary Material

Nanoscale distribution of TLR4 on primary human macrophages stimulated with LPS and ATI

Jan Neumann[a,b], Kira Ziegler[a], Márton Gelléri[b], Janine Fröhlich-Nowoisky[a], Fobang Liu[a], Iris Bellinghausen[c], Detlef Schuppan[d,e], Udo Birk[b,†], Ulrich Pöschl[a], Christoph Cremer[b,a], and Kurt Lucas[a]

[a]*Multiphase Chemistry Department, Max Planck Institute for Chemistry, Hahn-Meitner-Weg 1, 55128 Mainz, Germany*

[b]*Institute of Molecular Biology, Ackermannweg 4, 55128 Mainz, Germany*

[c]*Department of Dermatology, University Medical Center of the Johannes Gutenberg University, 55131 Mainz, Germany*

[d]*Institute of Translational Immunology, University Medical Center of the Johannes Gutenberg University, Langenbeckstraße 1, 55131 Mainz, Germany*

[e]*Division of Gastroenterology, Beth Israel Deaconess Medical Center, Harvard Medical School, 330 Brookline Ave, Boston, MA 02215, USA*

Correspondence to K. Lucas (k.lucas@mpic.de)

[†]Current address: Hochschule für Technik und Wirtschaft Chur, Pulvermühlestrasse 57, 7000 Chur, Switzerland

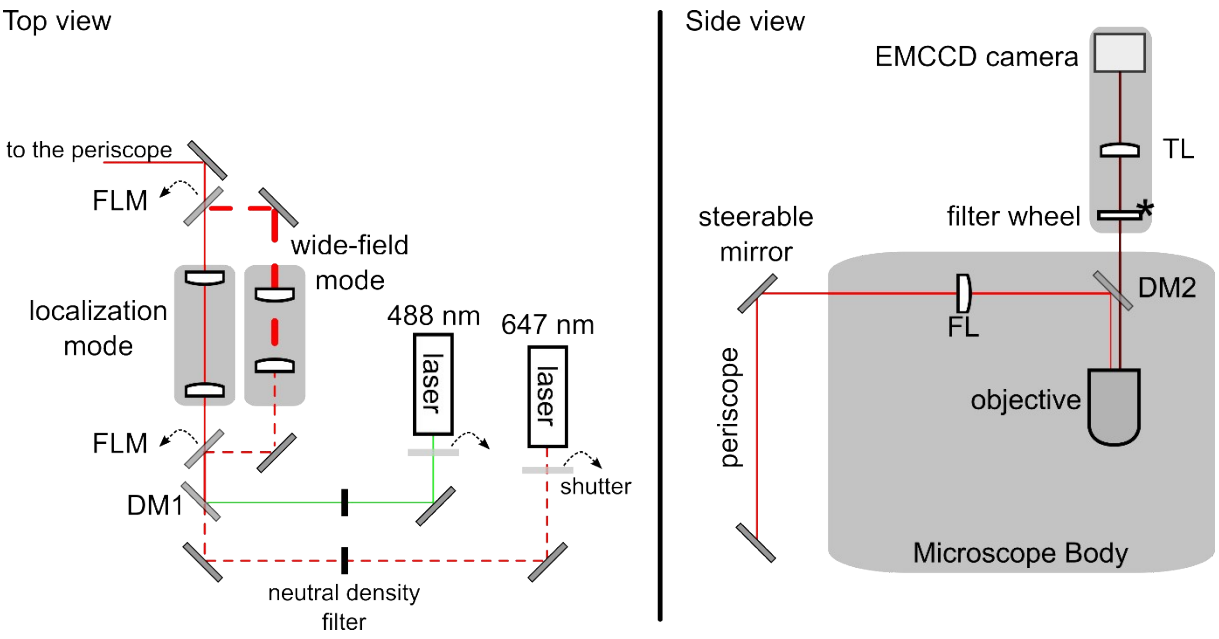

Fig. S1: Schematic diagram of the custom-built localization microscope setup. The setup was equipped with a 647 nm laser (Obis, Coherent) and a 488 nm laser (Sapphire, Coherent). Selection of laser lines was done with custom-built shutters and neutral density filters allowed adjustment of laser intensities. Both laser lines were combined using a dichromatic mirror (DM1; HC BS 580, AHF Analysetechnik). With two motorized flipping mirrors (FLM; Radiant Dyes), the laser beam could be switched between two beam paths consisting of beam expanders for localization or wide-field acquisitions. In wide-field mode, the laser beam was expanded 10-fold, illuminating the whole field of view of the camera (49.15 µm x 49.15 µm) homogenously. For localization measurements, the beam was expanded 3.125-fold. This led to an illuminated area of ~640 µm² in the sample plane (area derived from $1/e^2$ width of Gaussian profile). The collimated laser beams were coupled into the back port of the microscope (DM RBE, Leica) using a periscope. The mirror in the top unit was placed in the focal plane of the focusing lens and piezoelectric actuators (Thorlabs) attached to the mirror allowed the beam to be steered between epi-illumination and total internal reflection (TIR) illumination. The collimated laser beam was focused on the back focal plane of a 100x/NA 1.49 objective lens (Olympus) using a f = 300 mm focusing lens (FL, Thorlabs) mounted on a xyz-translator. The objective lens was attached to a piezo objective scanner (Physik Instrumente) for z-focusing of the sample. The sample was mounted on a xy-stepper stage, guided by a commercial controller (Corvus-2 eco TT, ITK Dr. Kassen GmbH). Fluorescence discrimination was done with a dichroic mirror (dual line zt488/647 rpc, AHF Analysetechnik) incorporated into a filter cube (DM2).

The filter cube also contained a laser clean-up filter (ZET488/640, AHF Analysetechnik) and a dual-notch filter (488/647 nm, AHF Analysetechnik) to remove remaining excitation light. Emitted fluorescent light was collected on an EMCCD camera (iXon 897 Ultra, Andor Technology) mounted on a custom-built camera adapter, which included an emission filter wheel. The emission filter wheel contained a 500 nm long pass filter (Chroma Technology) for 488 nm illumination and a 700/75 nm bandpass filter for 647 nm illumination. For astigmatism-based 3D localization microscopy,[1] a weak cylindrical lens (f = 1,000 mm, Thorlabs) could be placed between the tube lens (TL; f = 300 mm, Thorlabs) and the camera. Interfacing with all hardware devices and data acquisitions was done with μManager.[2]

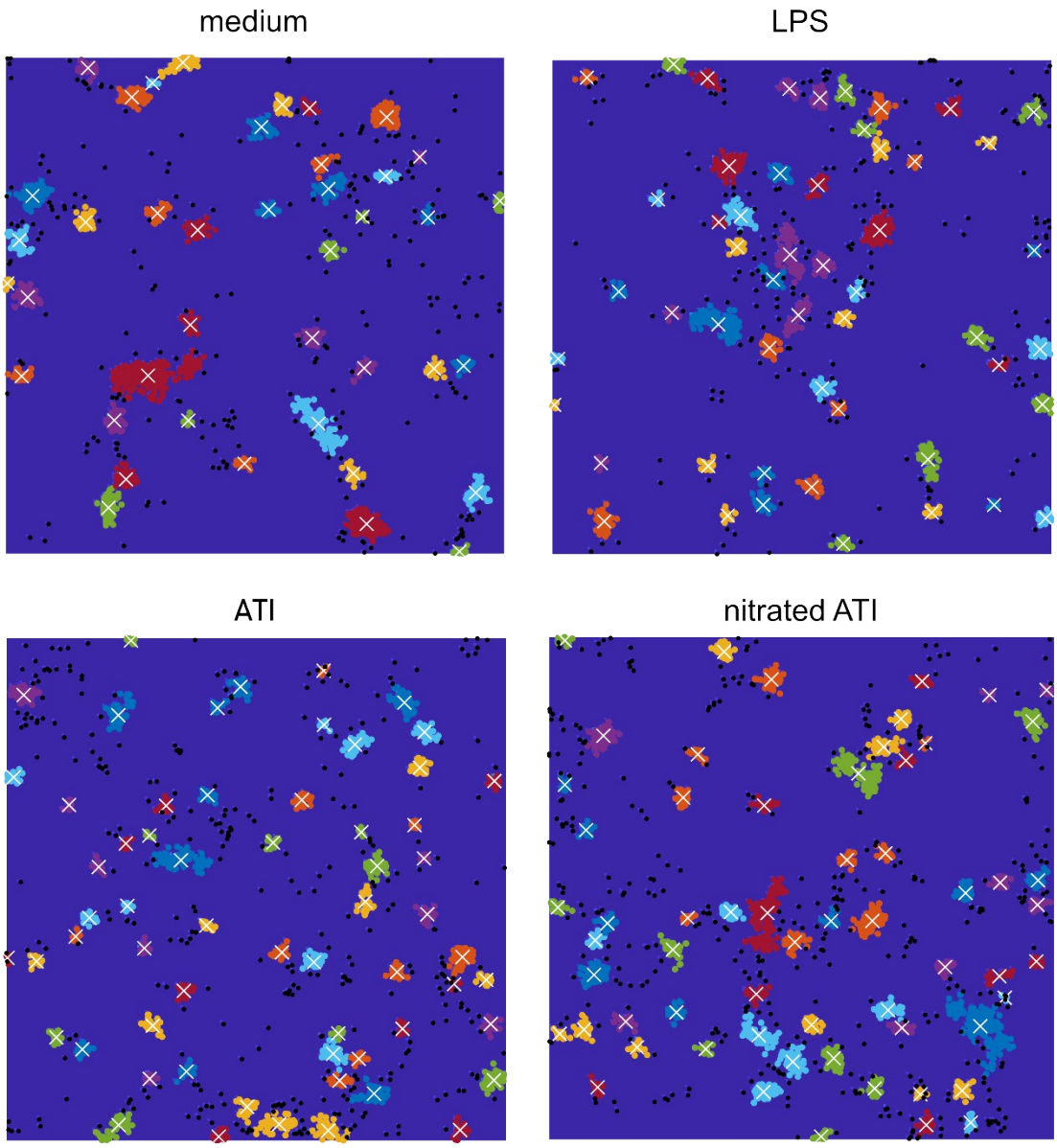

Fig. S2: Visualization of clusters as detected by DBSCAN. Representation of the detected clusters from the SMLM images from Fig. 1C. A color was randomly assigned to each identified cluster. The white cross indicates the center of mass of the cluster. Black dots represent detected molecules that are not part of a cluster.

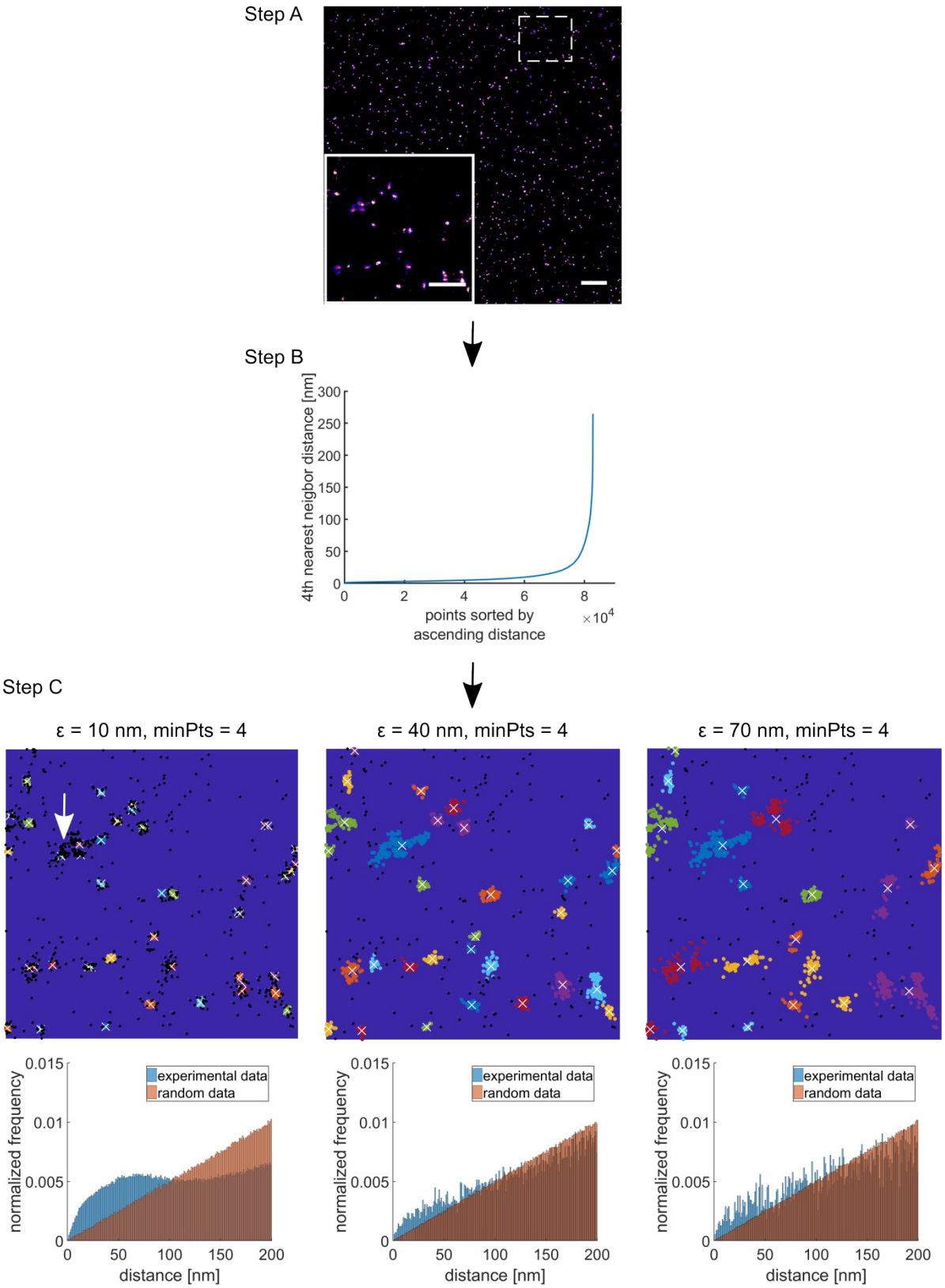

Fig. S3: Iterative determination of DBSCAN parameters. Different TLR4 sample data sets were selected for determination of DBSCAN parameters. Step A shows an 11.6 µm x 11.6 µm SMLM image from such a dataset containing approximately 80,000 detected single molecule signals (scale bar = 1 µm, inset scale bar = 500 nm). To

estimate the DBSCAN parameters (minPts and ε), a similar approach as shown in Ester et al (1996)[3] was used in a first step. The detected molecule coordinates from the list of localizations were used to determine the 4th nearest neighbor distances. These distances were sorted in ascending order and plotted against the number of detected signals. The distance value where the first strong bend in the curve occurs, was taken as a starting point for ε (step B, indicated by the black arrow). Next, DBSCAN was applied using minPts = 4 and the estimated ε obtained from step B. The clusters obtained by DBSCAN were visualized (step C). Every detected cluster is represented by a different color. Black dots correspond to molecules that are not part of a cluster or which belong to a cluster with a diameter larger than 1 µm. The white cross indicates the center of mass of the cluster. For better visibility, only the ROI from step A is shown, but calculations were done for all molecule signals of the dataset. In addition to the visualization, distances between all molecule signals outside of the detected clusters were calculated and plotted in a histogram (blue histogram). The obtained frequency distribution of distances was then compared to the one expected from a random distribution. To account for edge effects, distances originating from molecule signals that are located within the cut-off distance of 200 nm from the image border, were not calculated. The result of different combinations of ε and fixed minPts for DBSCAN is depicted in step C. Using an ε value of 10 nm, DBSCAN identified some small clusters that are surrounded by non-clustered molecule signals (assigned as noise, white arrow). By visual inspection, it appears that these noise signals belong to the clusters. This can be also seen in the frequency distribution of the distances from the molecule signals outside of the cluster (= noise points). At shorter distances, points deviate from the random distribution indicating clustering. If parameter for DBSCAN were correctly selected, these molecule signals should follow a random distribution. As a result, the ε parameter was set in this case to small. If ε is set to 40 nm, more molecule signals are assigned to a cluster and the frequency distribution of the distances from the residual noise signals approximates a random distribution. If ε is set too large, i.e. 70 nm, well separated clusters will be detected as one large cluster. The final parameters were found by iteratively adjusting minPts and ε such that the frequency distribution of distances from molecule signals outside of a cluster approximates a random distribution, supported by visual inspection of the clusters obtained from DBSCAN.

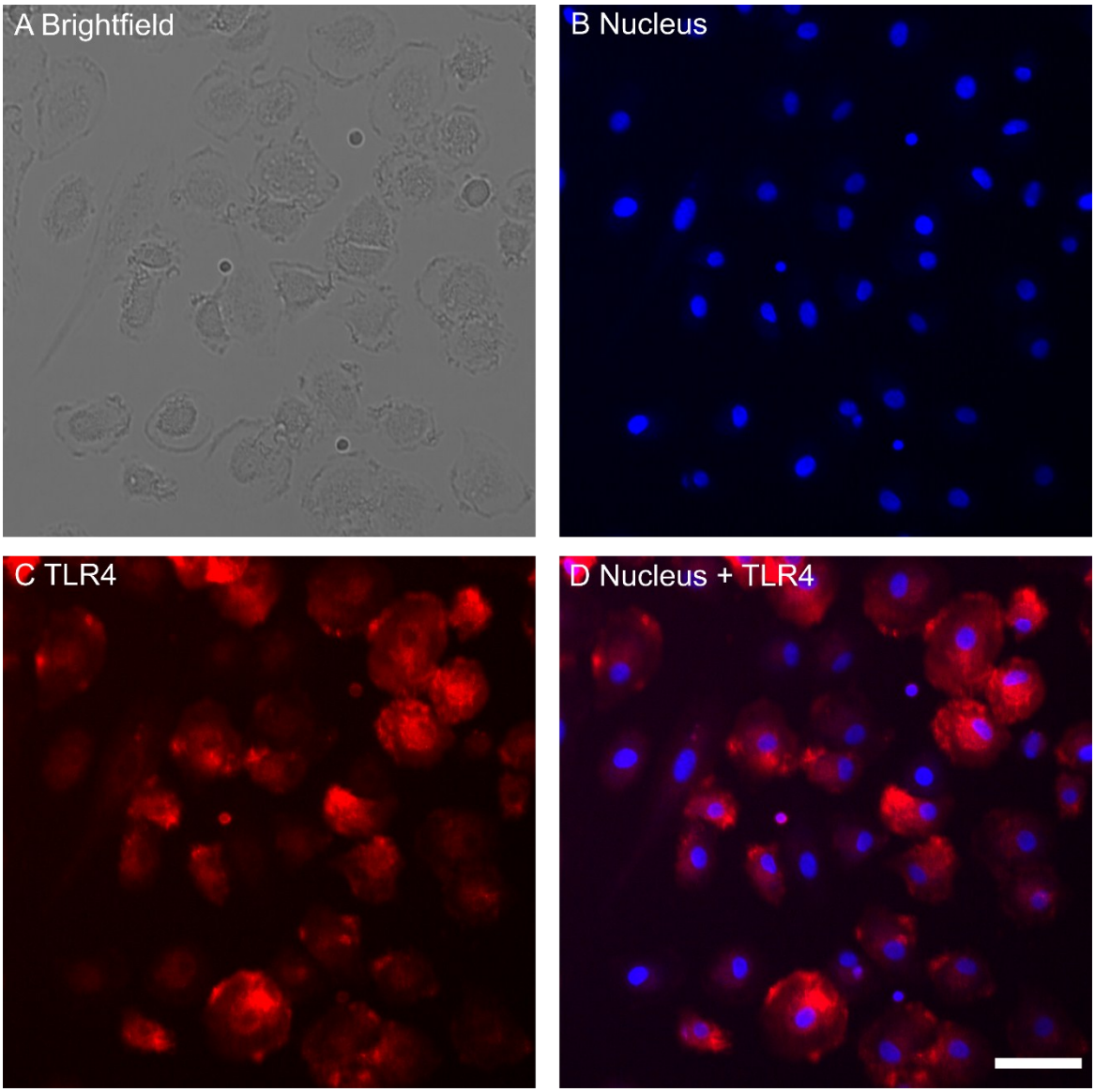

Fig. S4: Wide-field images of untreated primary human macrophages. Bright field (**A**) and fluorescence microscopy images of macrophages stained for the cell nucleus (**B**, pseudocolor blue) and TLR4 (**C**, pseudocolor red). (**D**) Overlay of nucleus and TLR4 image. Scale bar = 50 µm.

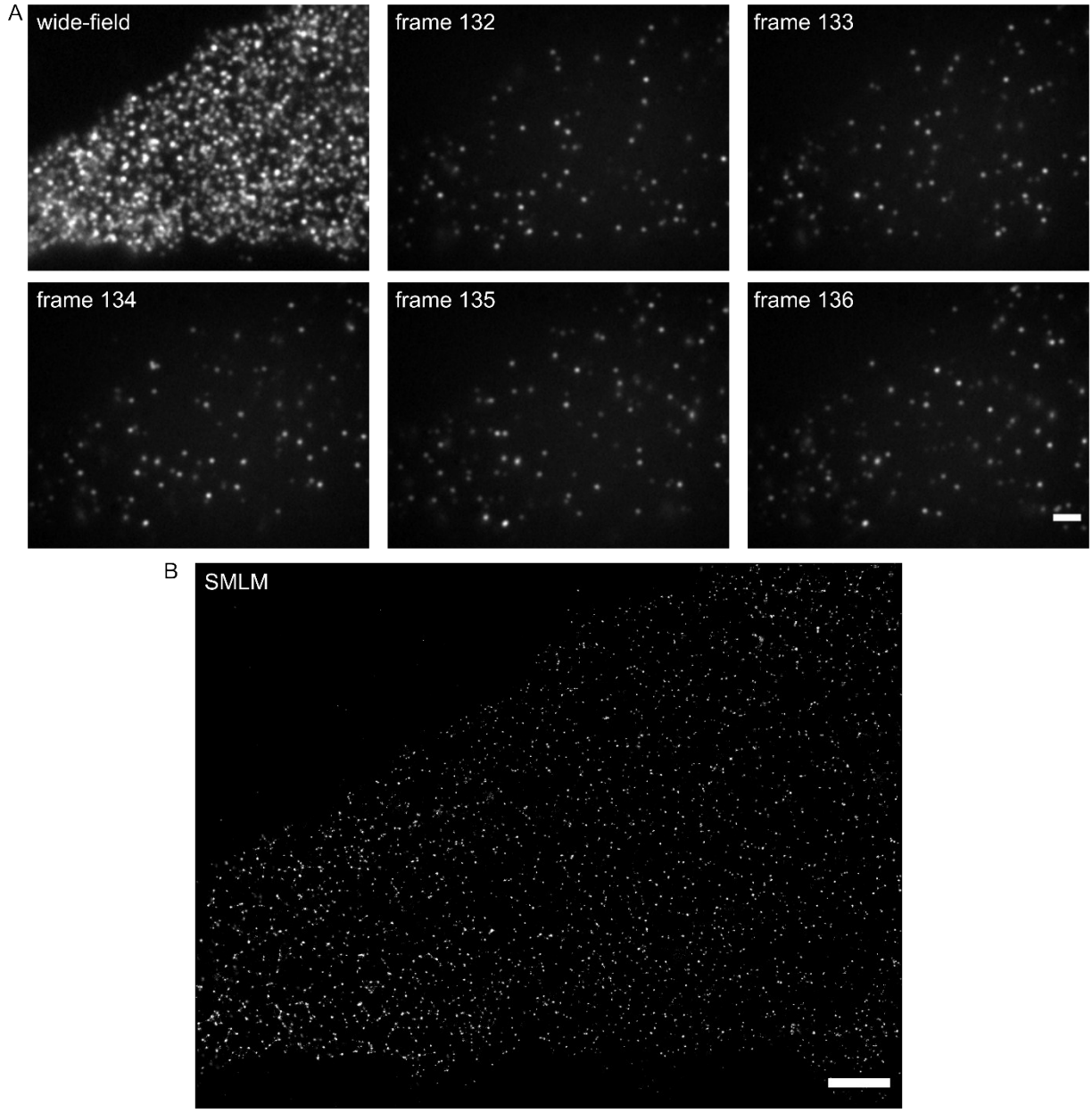

Fig. S5: Raw data images of the cell membrane of a TLR4 stained macrophage. (**A**) Wide-field image and frames 132 to 136 of the raw SMLM image data stack. A total of 5,000 frames was recorded for each cell. Scale bar = 2 µm. (**B**) Reconstructed SMLM image, where each detected signal had been blurred with a Gaussian function whose standard deviation is equal to the localization precision of the corresponding signal. Scale bar = 2 µm.

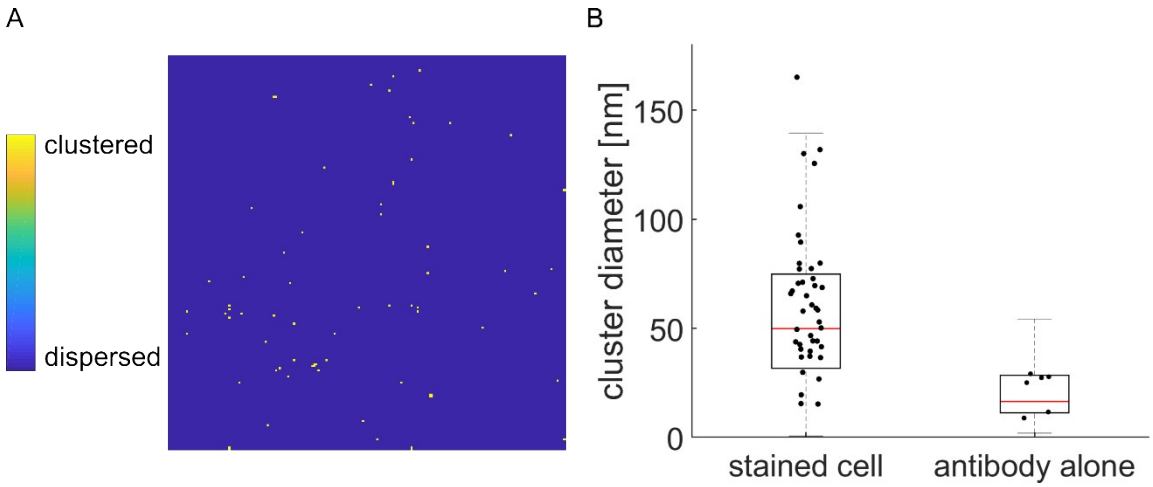

Fig. S6: Cluster size due to multiple blinking of the same fluorophore. (**A**) Grid-based density analysis of sparsely distributed secondary antibodies on a coverslip. 2 µm x 2 µm region of interest (ROI) showing the level of clustering. Yellow areas indicate clusters on the order of a few pixels. The pixel size is 10 nm. (**B**) Average cluster diameter obtained by DBSCAN. Every point corresponds to the average cluster diameter obtained from a stained cell or a field of sparsely distributed secondary antibodies on a coverslip (antibody alone). Of note, the cluster diameter obtained from the stained cell is the result of using a labeling system consisting of primary and secondary antibody. Furthermore, the mean localization precision in the cell sample was about 11 nm, whereas the mean localization precision in the antibody sample was about 16 nm. This could adversely influence the cluster diameter measured for the antibody sample.

Supplementary Note 1: Sample preparation to estimate size of clusters due to multiple blinking.

To estimate the size of clustering due to multiple blinking of the same fluorophore, coverslips containing sparsely distributed secondary antibodies were prepared. Glass coverslips (R. Langenbrinck GmbH) were coated with poly-l-lysine (Sigma Aldrich) for 15 min to 30 min and then rinsed in ddH_2O. Meanwhile, secondary antibodies (A-21237, Thermo Fisher Scientific) were diluted 1 to 10,000 in ddH_2O. After vortexing, 100 µl of diluted antibody solution were pipetted on parafilm. The coverslip was placed on top of it with the coated side facing downwards. The sample was incubated for 1 h to 2 h. Next, the sample was rinsed with PBS (Thermo Fisher Scientific), embedded in Vectashield H-1000 (Vector Laboratories) and sealed using picodent twinsil (picodent

Dental Produktions- und Vertriebs GmbH). Imaging and data evaluation were performed in the same way as for the cell samples.

Supplementary Note 2: Choice of stimulation time

The chosen stimulation times are based on previous studies with LPS as agonist, where it was shown that within 10 min after stimulation TLR4 is recruited into lipid rafts.[4] Furthermore, it was observed that TLR4 co-localizes with endosomes within 15 min of LPS stimulation.[5] Additionally, our measurements on macrophages revealed, that an LPS-induced translocation of NF-κB from the cytoplasm into the nucleus occurs within 30 minutes of stimulation (Fig. S7).

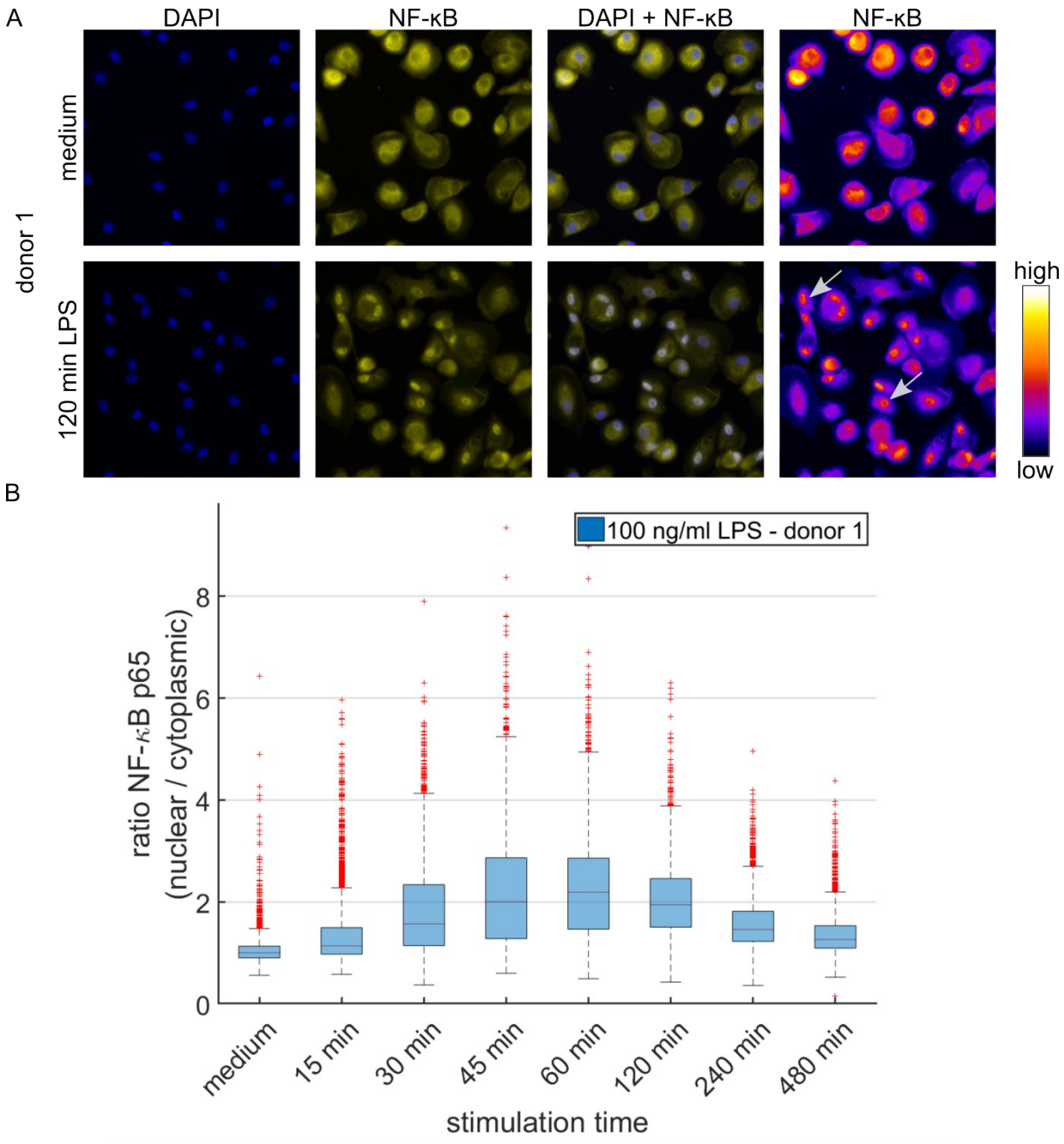

Fig. S7: Time-dependent translocation of NF-κB induced by LPS. (**A**) Fluorescence microscopy images of human primary macrophages stimulated for 120 min with LPS-EB (100 ng/ml). After fixation, cells were stained for NF-κB (pseudocolor yellow). The nucleus is counterstained using DAPI (pseudocolor blue). In the medium control NF-κB is mostly located in the cytoplasm, whereas in LPS-stimulated samples NF-κB is enriched in the nucleus (indicated by arrows). Scale bar = 50 µm. (**B**) Quantitative evaluation of NF-κB translocation for cells fixed at indicated time points. The ratio of nuclear to cytoplasmic NF-κB is plotted against the stimulation time. Nuclear translocation of NF-κB is visible within 30 min of LPS stimulation.

Supplementary Note 3: Treatment, immunofluorescence staining and imaging of NF-κB p65.

Treatment

Primary human macrophages were isolated and differentiated as described in the experimental section. Cells were seeded on 12-well glass bottom plates (Cellvis). After 6 days of differentiation, cells were stimulated with 100 ng/ml LPS-EB for 15 min to 480 min. Cells were then washed once in pre-warmed PBS and subsequently fixed using 4 % formaldehyde in PBS for 10 min at 37 °C. Next, cells were washed three times in PBS before proceeding with immunostaining of NF-κB.

Immunofluorescence staining

For immunostaining, cells were permeabilized and blocked for 1 h in PBS containing 5 % bovine serum albumin (BSA; Cell Signaling Technology) and 0.3 % Triton X-100 (Merck). Primary antibody (D14E12, Cell Signaling Technology), directed against human p65 subunit of NF-κB, was diluted 1 to 400 in antibody dilution buffer (1 % BSA and 0.3 % Triton X-100 in PBS). Cells with primary antibody were incubated overnight at 4 °C. Afterwards, cells were washed three times in PBS, followed by incubation with goat anti-rabbit Alexa Fluor 568 conjugated secondary antibody (Thermo Fisher Scientific, cat. no. A-11011), diluted 1 to 400 in the same buffer as the primary antibody. After 1 h of incubation at room temperature, cells were again washed three times in PBS. Counterstaining of cell nuclei was done using 4’,6-diamidino-2-phenylindole (DAPI; Thermo Fisher Scientific) at a concentration of 300 nM in PBS for 3 min. After three washing steps in PBS, stained cells were immediately imaged. PBS was used as the imaging buffer.

Imaging

Imaging was done using the Opera Phenix High-Content Screening system (PerkinElmer). Samples were imaged through a 20x/1.0 water immersion objective. Cells stained for NF-κB p65 and DAPI were excited using 561 nm and 405 nm laser lines, respectively. Emitted light was collected on two sCMOS cameras through specific emission filters for NF-κB p65 (570 nm to 630 nm) and DAPI (435 nm to 480 nm). 2 x 2 binning was used for the two cameras and the microscope was operated in

a non-confocal mode. Intensity and exposure time were set to obtain sub-saturating pixels. In each well, images from 72 different ROIs were taken.

Image processing was done using Harmony software (PerkinElmer). First, stained cell nuclei were identified by segmenting the DAPI channel. Identified nuclei were used as seeds to identify their corresponding cytoplasm masks using the NF-κB p65 channel. Masks were resized to avoid overlapping between them and to stay within the boundaries of the cell. Finally, a nuclear mask with a corresponding ring-like cytoplasm mask was obtained. Mean NF-κB p65 intensities within both masks were determined and the ratio of nuclear to cytoplasmic NF-κB p65 was calculated.

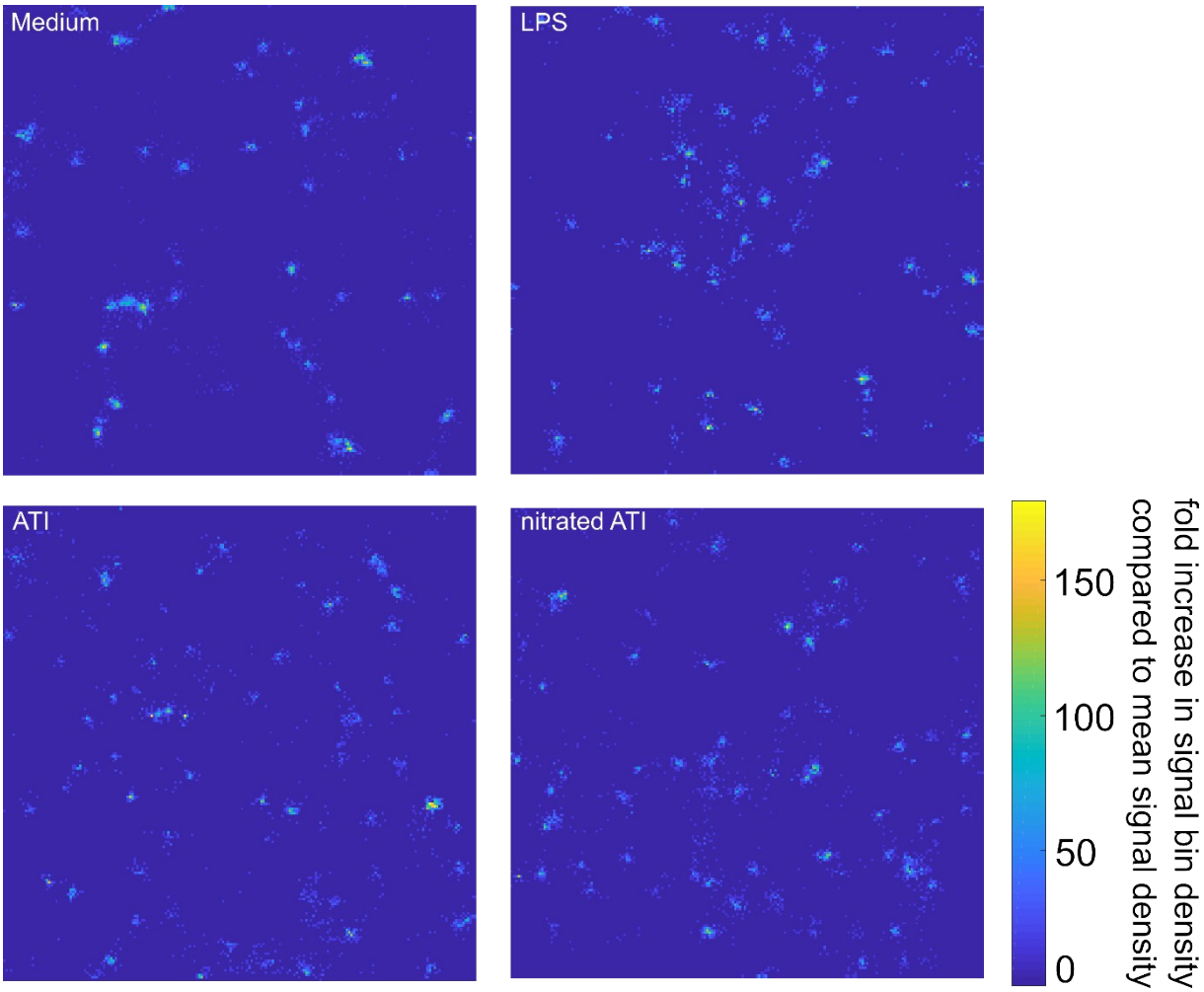

Fig. S8: Grid-based density analysis reveals the local level of clustering. Representation of the grid-based density analysis depicted in Figure 1D with absolute values. Detected signals were binned on a 10 nm x 10 nm grid and the signal density of each bin was divided by the mean signal density of the corresponding ROI.

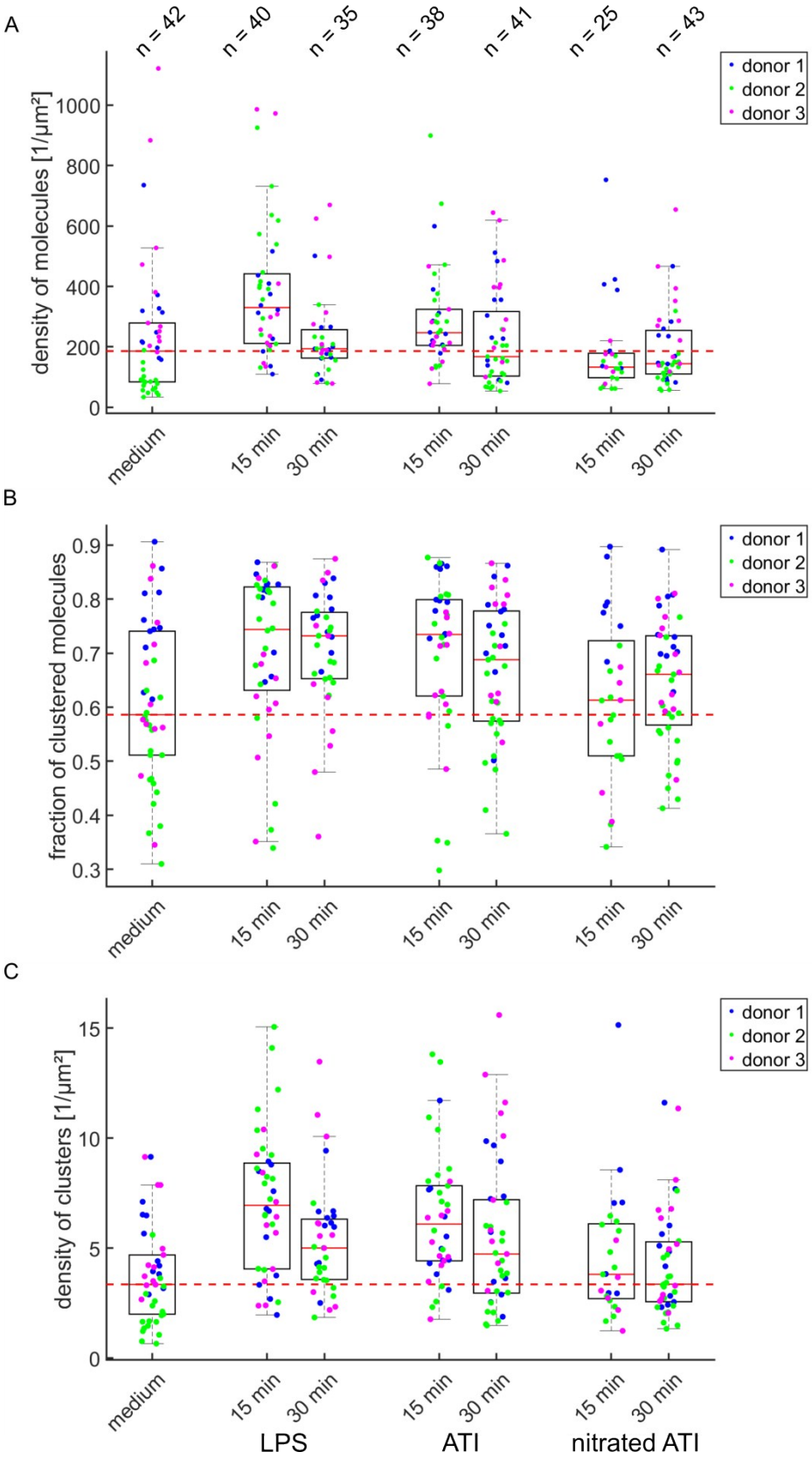

Fig. S9: TLR4 membrane clustering upon LPS and ATI stimulation. The mean density of detected molecules on the cell membrane (**A**) as well as the fraction of clustered molecules (**B**) and the density of clusters (**C**) as analyzed by DBSCAN is shown. The boxes represent the median and the 25th to 75th percentile, whereas the

whiskers cover 99.3 % of the data. The horizontal red line indicates the median value of the medium control. Overlaid dots represent mean values obtained from different cells. The color of the dots corresponds to the respective donors and the number above each treatment denotes the number of measured cells.

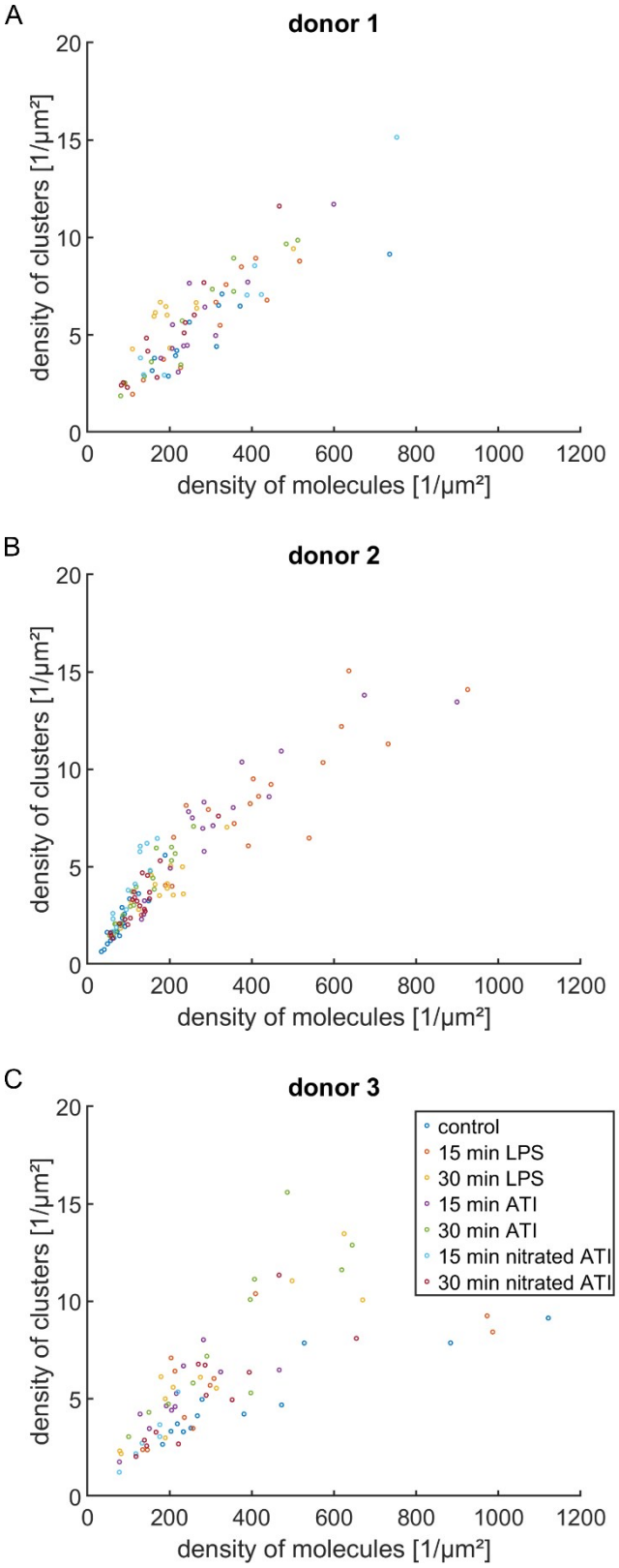

Fig. S10: Correlation between TLR4 surface representation and TLR4 clustering. For donor 1 (A), donor 2 (B) and donor 3 (C) the density of molecules vs. the density of clusters on the cell membrane is shown. All plots indicate a positive correlation between both variables. Each point represents a cell and the color of the point corresponds to the respective treatment.

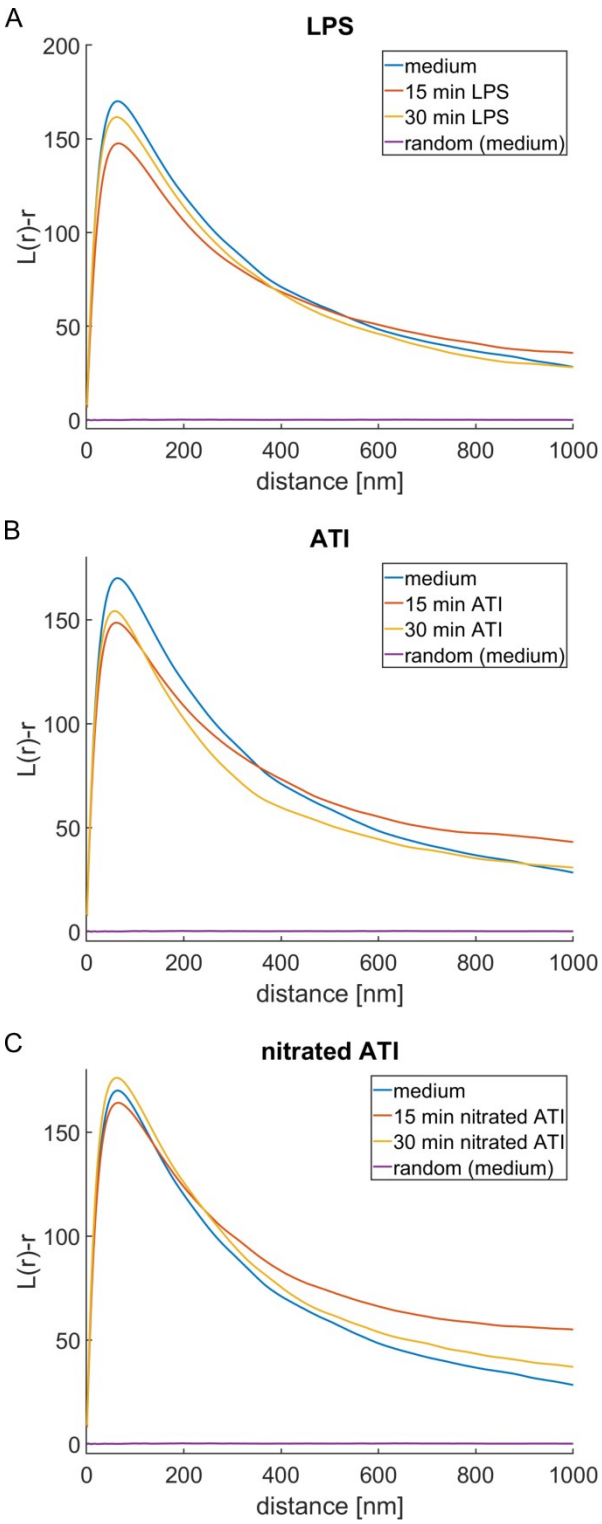

Fig. S11: Average of Ripley's H-function for the different treatments. Ripley's H-function of macrophages stimulated for 15 min and 30 min with (**A**) 100 ng/ml LPS, (**B**) 12.5 µg/ml ATI or (**C**) 12.5 µg/ml nitrated ATI. Each function displays the average obtained from three healthy donors. All plots also show Ripley's H-function, which was obtained from the random data of the medium sample.

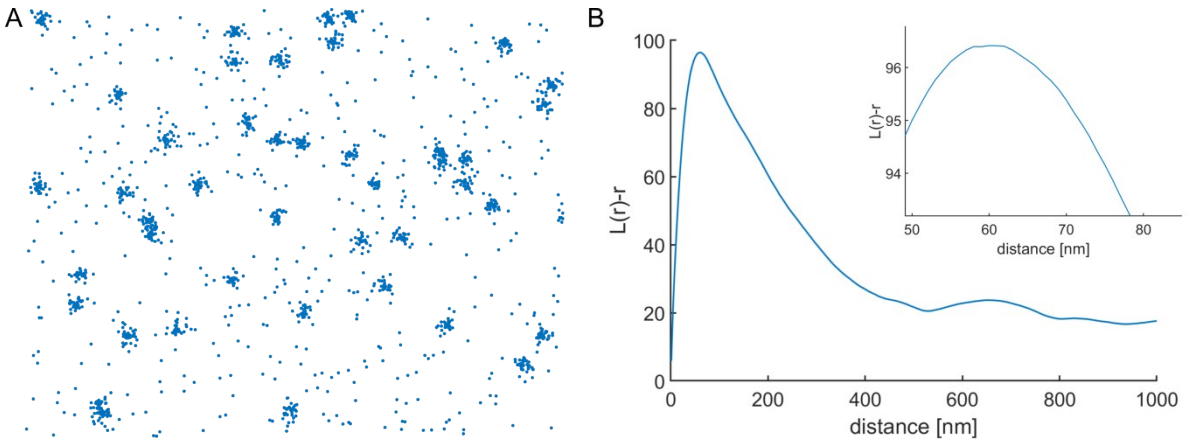

Fig. S12: Simulation of clusters. (**A**) Section of a 10 µm x 10 µm simulated image. Simulation parameters were set to represent experimental data. The average density is 300 molecule signals/µm², with 70 % of molecule signals being part of a simulated Gaussian-shaped cluster. Simulated clusters were randomly distributed over the randomly simulated point pattern with an average density of 6 cluster/µm². Cluster diameter was set to 60 nm. (**B**) Ripley's H-function of the simulated point pattern. The maximum of Ripley's function is approximately 60 nm.

Table S1: TLR4 cluster size obtained by Ripley's H-function. Values denote mean ± standard deviation.

	donor	number of cells	Maximum Ripley's H function [nm]
medium	donor 1	11	58 ± 5
	donor 2	19	67 ± 11
	donor 3	12	66 ± 9
15 min LPS	donor 1	11	66 ± 15
	donor 2	18	62 ± 14
	donor 3	10	75 ± 44
30 min LPS	donor 1	11	58 ± 8
	donor 2	13	64 ± 7
	donor 3	11	67 ± 29
15 min ATI	donor 1	11	61 ± 10
	donor 2	16	69 ± 37
	donor 3	11	62 ± 15
30 min ATI	donor 1	11	64 ± 10
	donor 2	19	55 ± 7
	donor 3	11	51 ± 5
15 min nitrated ATI	donor 1	7	62 ± 8
	donor 2	12	53 ± 8
	donor 3	6	79 ± 25
30 min nitrated ATI	donor 1	11	58 ± 9
	donor 2	20	58 ± 10
	donor 3	12	65 ± 14

	number of cells			density of molecules on the membrane [1/µm²]			fraction of clustered molecules			number of molecules per cluster		
Buffycoat	Donor 1	Donor 2	Donor 3	Donor 1	Donor 2	Donor 3	Donor 1	Donor 2	Donor 3	Donor 1	Donor 2	Donor 3
medium	11	19	12	300 ± 160	80 ± 40	420 ± 300	0.7 ± 0.1	0.5 ± 0.1	0.6 ± 0.1	48 ± 46	21 ± 19	59 ± 87
15 min LPS	11	18	11	300 ± 130	430 ± 210	380 ± 300	0.8 ± 0.1	0.7 ± 0.2	0.6 ± 0.1	44 ± 42	37 ± 45	54 ± 99
30 min LPS	11	13	11	210 ± 110	190 ± 65	300 ± 210	0.8 ± 0.1	0.7 ± 0.1	0.7 ± 0.2	28 ± 26	31 ± 30	40 ± 47
15 min ATI	11	16	11	280 ± 120	340 ± 200	230 ± 105	0.8 ± 0.1	0.7 ± 0.2	0.7 ± 0.1	39 ± 34	33 ± 47	30 ± 36
30 min ATI	11	19	11	270 ± 150	130 ± 60	360 ± 180	0.7 ± 0.1	0.6 ± 0.1	0.7 ± 0.1	37 ± 37	23 ± 21	32 ± 35
15 min nitrated ATI	7	12	6	350 ± 220	110 ± 40	150 ± 50	0.8 ± 0.1	0.5 ± 0.1	0.6 ± 0.1	43 ± 42	15 ± 12	29 ± 31
30 min nitrated ATI	11	20	12	200 ± 110	120 ± 60	290 ± 160	0.7 ± 0.1	0.6 ± 0.1	0.7 ± 0.1	30 ± 28	23 ± 20	42 ± 57

	cluster diameter [nm]			density of molecules within clusters [x10^4 1/µm²]			distance to next neighboring cluster [nm]			density of clusters [1/µm²]		
Buffycoat	Donor 1	Donor 2	Donor 3	Donor 1	Donor 2	Donor 3	Donor 1	Donor 2	Donor 3	Donor 1	Donor 2	Donor 3
medium	57 ± 29	38 ± 20	65 ± 41	2.3 ± 16	2.4 ± 4.3	2.1 ± 23	230 ± 120	360 ± 230	230 ± 120	5 ± 2	2 ± 1	5 ± 2
15 min LPS	57 ± 27	52 ± 32	59 ± 43	1.9 ± 4.5	2.0 ± 2.7	2.0 ± 2.6	220 ± 110	190 ± 90	230 ± 130	6 ± 3	8 ± 3	6 ± 3
30 min LPS	43 ± 24	46 ± 25	55 ± 32	2.4 ± 4.6	2.4 ± 3.9	1.9 ± 2.0	220 ± 120	270 ± 150	200 ± 110	6 ± 2	4 ± 1	6 ± 3
15 min ATI	53 ± 25	48 ± 32	45 ± 27	2.1 ± 17	3.3 ± 85	2.5 ± 3.6	220 ± 120	200 ± 120	230 ± 130	6 ± 3	8 ± 3	5 ± 2
30 min ATI	52 ± 28	39 ± 22	46 ± 24	2.1 ± 7.3	2.7 ± 5.3	2.2 ± 1.9	230 ± 130	260 ± 150	190 ± 100	6 ± 3	4 ± 2	8 ± 4
15 min nitrated ATI	58 ± 29	31 ± 16	45 ± 27	1.7 ± 1.5	2.9 ± 4.1	2.4 ± 2.7	200 ± 110	260 ± 160	290 ± 170	7 ± 4	4 ± 2	3 ± 1
30 min nitrated ATI	47 ± 26	39 ± 21	56 ± 34	2.5 ± 19	3.1 ± 23	2.1 ± 4.7	240 ± 140	300 ± 180	240 ± 140	5 ± 3	3 ± 2	5 ± 3

Table S2: Donor-specific results from TLR4's density-based clustering analysis. Values denote mean ± standard deviation.

	number of cells	density of molecules on the membrane [1/µm²]	fraction of clustered molecules	number of molecules per cluster
medium	42	240 ± 230	0.6 ± 0.2	48 ± 68
15 min LPS	40	380 ± 220	0.7 ± 0.1	43 ± 62
30 min LPS	35	230 ± 140	0.7 ± 0.1	33 ± 37
15 min ATI	38	290 ± 160	0.7 ± 0.1	34 ± 41
30 min ATI	41	230 ± 160	0.7 ± 0.1	31 ± 32
15 min nitrated ATI	25	180 ± 160	0.6 ± 0.1	31 ± 35
30 min nitrated ATI	43	190 ± 130	0.6 ± 0.1	31 ± 38

	cluster diameter [nm]	density of molecules within clusters [x10^4 1/µm²]	distance to next neighboring cluster [nm]	density of clusters [1/µm²]
medium	57 ± 36	2.2 ± 19	260 ± 150	4 ± 2
15 min LPS	55 ± 34	2.0 ± 3.3	200 ± 110	7 ± 3
30 min LPS	48 ± 28	2.2 ± 3.6	230 ± 130	5 ± 3
15 min ATI	49 ± 29	2.7 ± 57	220 ± 120	6 ± 3
30 min ATI	46 ± 25	2.3 ± 5.3	230 ± 130	6 ± 3
15 min nitrated ATI	47 ± 28	2.2 ± 2.8	240 ± 140	5 ± 3
30 min nitrated ATI	47 ± 28	2.6 ± 18	260 ± 150	4 ± 2

Table S3: Averaged results from TLR4's density-based clustering analysis. Values denote mean ± standard deviation.

References

1 B. Huang, W. Wang, M. Bates and X. Zhuang, *Science*, 2008, **319**, 810–813.

2 A. Edelstein, N. Amodaj, K. Hoover, R. Vale and N. Stuurman, *Curr. Protoc. Mol. Biol.*, 2010, **92**, 1–17.

3 M. Ester, H.-P. Kriegel, J. Sander and X. Xu, *Proc. Second Int. Conf. Knowl. Discov. Data Min.*, 1996, 226–231.

4 J. Cuschieri, E. Bulger, J. Billgrin, I. Garcia and R. V. Maier, *Surg. Infect. (Larchmt).*, 2007, **8**, 91–106.

5 H. Husebye, Ø. Halaas, H. Stenmark, G. Tunheim, Ø. Sandanger, B. Bogen, A. Brech, E. Latz and T. Espevik, *EMBO J.*, 2006, **25**, 683–692.